



Universiteit
Leiden
The Netherlands

Synthesis and structural analysis of *Aspergillus fumigatus* galactosaminogalactans featuring α -galactose, α -galactosamine and α -N-acetyl galactosamine linkages

Codée, J.D.C.; Zhang, Y.; Gómez-Redondo, M.; Jiménez-Osés, G.; Arda, A.; Overkleeft, H.S.; ... ; Jiménez-Barbero, J.

Citation

Codée, J. D. C., Zhang, Y., Gómez-Redondo, M., Jiménez-Osés, G., Arda, A., Overkleeft, H. S., ... Jiménez-Barbero, J. (2020). Synthesis and structural analysis of *Aspergillus fumigatus* galactosaminogalactans featuring α -galactose, α -galactosamine and α -N-acetyl galactosamine linkages. *Angewandte Chemie International Edition*, 59(31), 12746-12750. doi:10.1002/anie.202003951

Version: Publisher's Version

License: [Licensed under Article 25fa Copyright Act/Law \(Amendment Taverne\)](#)

Downloaded from: <https://hdl.handle.net/1887/3200735>

Note: To cite this publication please use the final published version (if applicable).

Oligosaccharides

Synthesis and Structural Analysis of *Aspergillus fumigatus* Galactosaminogalactans Featuring α -Galactose, α -Galactosamine and α -N-Acetyl Galactosamine Linkages

Yongzhen Zhang, Marcos Gómez-Redondo, Gonzalo Jiménez-Osés, Ana Arda, Herman S. Overkleeft, Gijsbert A. van der Marel, Jesús Jiménez-Barbero,* and Jeroen D. C. Codée*

Abstract: Galactosaminogalactan (GAG) is a prominent cell wall component of the opportunistic fungal pathogen *Aspergillus fumigatus*. GAG is a heteropolysaccharide composed of α -1,4-linked galactose, galactosamine and N-acetylgalactosamine residues. To enable biochemical studies, a library of GAG-fragments was constructed featuring specimens containing α -galactose-, α -galactosamine and α -N-acetyl galactosamine linkages. Key features of the synthetic strategy include the use of di-*tert*-butylsilylidene directed α -galactosylation methodology and regioselective benzylation reactions using benzoyl-hydroxybenzotriazole (Bz-OBt). Structural analysis of the Gal, GalN and GalNAc oligomers by a combination of NMR and MD approaches revealed that the oligomers adopt an elongated, almost straight, structure, stabilized by inter-residue H-bonds, one of which is a non-conventional C–H...O hydrogen bond between H5 of the residue ($i + 1$) and O3 of the residue (i). The structures position the C-2 substituents almost perpendicular to the oligosaccharide main chain axis, pointing to the bulk solvent and available for interactions with antibodies or other binding partners.

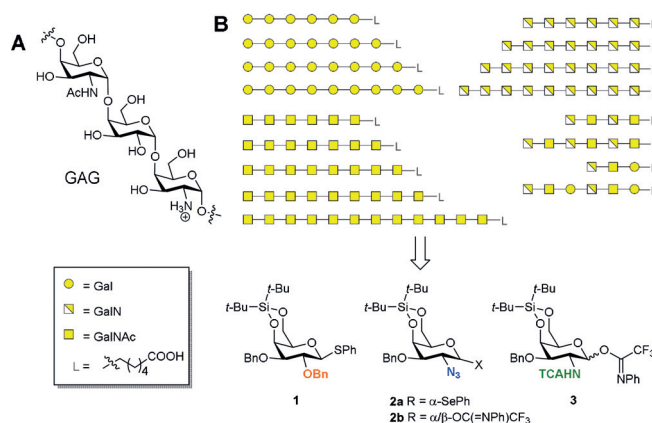
A *Aspergillus fumigatus* is an opportunistic pathogenic fungus that causes invasive infections in immunocompromised patients, with a mortality rate of 60–80%.^[1] Galactosaminogalactan (GAG), a prominent cell wall component of *A. fumigatus*, has been identified as an important factor during infection/invasion of the host.^[2] The GAG polysaccharide is composed of galactose (Gal), galactosamine (GalN) and N-

acetylgalactosamine (GalNAc) residues that are interconnected through 1,4-*cis*-glycosidic linkages and are distributed in a seemingly random order^[2b,3] (Figure 1 A). To unravel the mode of action of enzymes involved in GAG-biosynthesis, well-defined GAG-fragments are indispensable tools.^[4] Pure GAG-oligosaccharide fragments can also be employed to study their interaction with components of the host immune system and map interactions with antibodies at the molecular level. This can inspire the development of anti-fungal vaccines and diagnostics. The random distribution of the Gal, GalN- and GalNAc monosaccharides in the GAG chains impedes the isolation of pure and well-defined specimens from natural sources and therefore we set out to synthesize a library of structurally well-defined GAG-fragments (see Figure 1 B). Recently, Nifantiev and co-workers^[5] reported on the assembly of a set of GAG homo-oligomers up to the hexamer level, containing either GalN or GalNAc residues. Because enzymes involved in GAG biosynthesis may require longer oligosaccharides, we assembled structures up to the dodecasaccharide level. As the structural variation in GAGs will be important in the interaction with the host immune system as well as fungal biosynthesis enzymes, we developed chemistry to enable the assembly of hetero-oligosaccharides, containing α -Gal, α -GalN and α -GalNAc residues.

To generate structurally varying GAG structures we reasoned that Kiso's di-*tert*-butylsilylene (DTBS)-directed α -selective galactosylation methodology would be especially

[*] Y. Zhang, Prof. Dr. H. S. Overkleeft, Prof. Dr. G. A. van der Marel, Dr. J. D. C. Codée
Leiden Institute of Chemistry, Leiden University
Einsteinweg 55, 2333 CC Leiden (The Netherlands)
E-mail: jcodee@chem.leidenuniv.nl
M. Gómez-Redondo, Dr. G. Jiménez-Osés, Dr. A. Arda,
Prof. Dr. J. Jiménez-Barbero
CIC bioGUNE, Basque Research and Technology Alliance (BRTA)
Bizkaia Technology Park, Building 800, 48160 Derio, Bizkaia (Spain)
Prof. Dr. J. Jiménez-Barbero
Ikerbasque, Basque Foundation for Science
Maria Diaz de Haro 3, 48013 Bilbao (Spain)
and
Department Organic Chemistry II, Faculty Science & Technology,
EHU-UPV, Leioa (Spain)

Supporting information and the ORCID identification number(s) for the author(s) of this article can be found under <https://doi.org/10.1002/anie.202003951>.

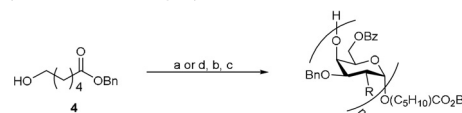


suited, as it gives unusual high α -stereoselectivity even when a C-2 group is present, that is capable of neighboring group participation.^[6] We thus designed donors **1**, **2** and **3** to assemble a library of GAG-structures, as depicted in Figure 1B. We incorporated a hexanoic acid spacer at the reducing end of the fragments for future conjugation purposes. The GalN₃ donor **2** will serve as precursor for GalN and GalNAc residues in the homo-oligomers as well as GalN residues in the hetero-oligosaccharides. The trichloroacetamide donor **3** will be used for the GalNAc moieties in the latter structures.

Table 1 summarizes the syntheses of the fully protected Gal- and GalN₃ homo-oligomers. The chain-elongation cycles consisted of the following steps: 1) glycosylation, 2) DTBS-removal, and 3) selective benzoylation of the primary alcohol group. For the latter transformation we used benzoyl-hydroxybenzotriazole (BzOBt) as a mild acylating agent to achieve the required regioselectivity.^[7]

As can be seen from the table, all glycosylations using the Gal-donor **1** proceeded efficiently providing the elongated sequences ($n=1-9$, R=OBn) with excellent stereoselectivity. Removal of the silyliden ketals and regioselective protection of the liberated C-6-hydroxyl groups also proceeded uneventfully and the efficiency of the chemistry did not diminish with growing chain length. For the assembly of the GalN/GalNAc homo-oligomers we first explored the use of selenophenyl donor **2a**. The relatively moderate yield of the glycosylation for the mono-, di- and trimer (R = N₃, 64% for **30**, 67% for **33** and 60% for **36**) however, forced us to switch to an alternative method and we therefore resorted to the use of *N*-phenyltrifluoroacetimidate donor **2b**.^[8] This donor performed well and all glycosylations proceeded effectively up to the dodecasaccharide level. Also here, the protecting group manipulations posed no problems and the desilylation and benzoylation reactions proceeded in excellent yields (84–96% and 90–94%, respectively) also on the large substrates. We next set out to assemble mixed sequences. Scheme 1A depicts the assembly of GalN₃-GalNTCA

Table 1: Synthesis of homopolymers of Gal and GalN₃.

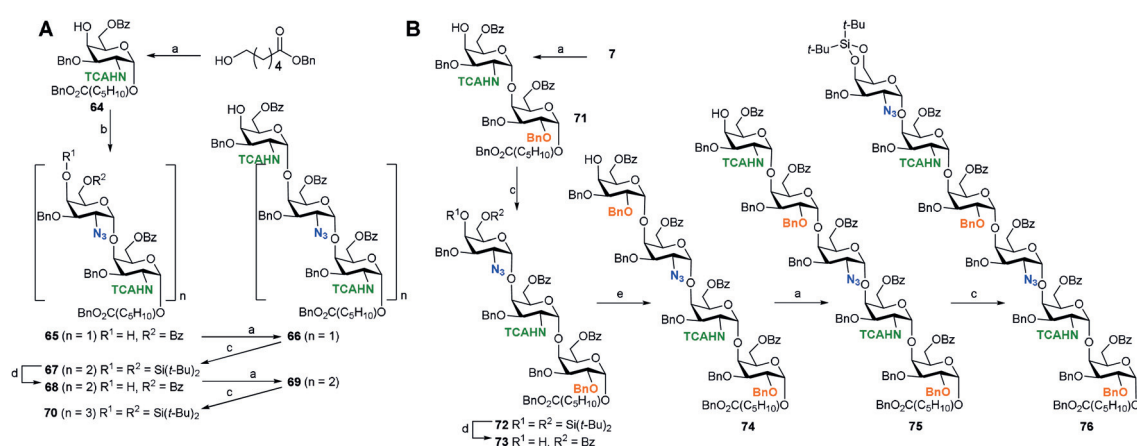


n	R	Glycosylation ^[a]	Desilylation ^[b]	Benzoylation ^[c]
1	OBn	5 (86%)	6 (92%)	7 (94%)
2	OBn	8 (91%)	9 (96%)	10 (95%)
3	OBn	11 (84%)	12 (94%)	13 (95%)
4	OBn	14 (80%)	15 (93%)	16 (92%)
5	OBn	17 (80%)	18 (92%)	19 (90%)
6	OBn	20 (72%)	21 (93%)	22 (95%)
7	OBn	23 (76%)	24 (95%)	25 (94%)
8	OBn	26 (81%)	27 (93%)	28 (95%)
9	OBn	29 (65%)	—	—
1	N ₃	30 (83%) (64%) ^[d]	31 (94%)	32 (93%)
2	N ₃	33 (91%) (67%) ^[d]	34 (95%)	35 (92%)
3	N ₃	36 (84%) (60%) ^[d]	37 (92%)	38 (94%)
4	N ₃	39 (82%)	40 (91%)	41 (92%)
5	N ₃	42 (90%)	43 (93%)	44 (90%)
6	N ₃	45 (89%)	46 (92%)	47 (90%)
7	N ₃	48 (88%)	49 (94%)	50 (92%)
8	N ₃	51 (87%)	52 (91%)	53 (94%)
9	N ₃	54 (89%)	55 (94%)	56 (90%)
10	N ₃	57 (65%)	58 (96%)	59 (94%)
11	N ₃	60 (73%)	61 (84%)	62 (93%)
12	N ₃	63 (79%)	—	—

[a] **1**, NIS, TFOH, 4 Å MS, DCM, 0°C; or **2b**, TFOH, 4 Å MS, DCM, 0°C.

[b] HF/pyridine, THF, rt. [c] BzOBt, Et₃N, DCM, rt. [d] **2a**, NIS, TFOH, 4 Å MS, DCM, 0°C.

oligomers, which started by condensation of 6-hydroxyhexanoic acid and GalNTCA-donor **3** (Scheme 1A). Even though donor **3** is equipped with a C-2-trichloroacetamide group, intrinsically capable of neighboring group participation, the α -linked product was selectively formed (94% yield, $\alpha/\beta=8:1$) when the reaction was performed at 0°C. Lowering the temperature to −20°C increased the selectivity to 14:1 (α /



Scheme 1. Synthesis of heteropolymers of Gal, GalN₃ and GalNTCA. a) i) **3**, TFOH, 4 Å MS, DCM, 0°C; ii) HF/pyridine (70%), THF, rt; iii) BzOBt, Et₃N, DCM, rt, yields (over 3 steps) for **64**: 70% or 69% (−20°C); for **66**: 76%; for **69**: 78%; for **71**: 78%; for **75**: 63%. b) i) **2b**, TFOH, 4 Å MS, DCM, 0°C, 92%; ii) HF/pyridine (70%), THF, rt, 93%; iii) BzOBt, Et₃N, DCM, rt, 94%. c) **2b**, TFOH, 4 Å MS, DCM, 0°C, for **67**: 91%; for **70**: 86%; for **72**: 86%; for **76**: 73%. d) i) HF/pyridine (70%), THF, rt; ii) BzOBt, Et₃N, DCM, rt, yields (over 2 steps) for **68**: 86%; for **73**: 88%. e) i) **1**, NIS, TFOH, 4 Å MS, DCM, 0°C, 87%; ii) HF/pyridine (70%), THF, rt, 97%; iii) BzOBt, Et₃N, DCM, rt, 92%.

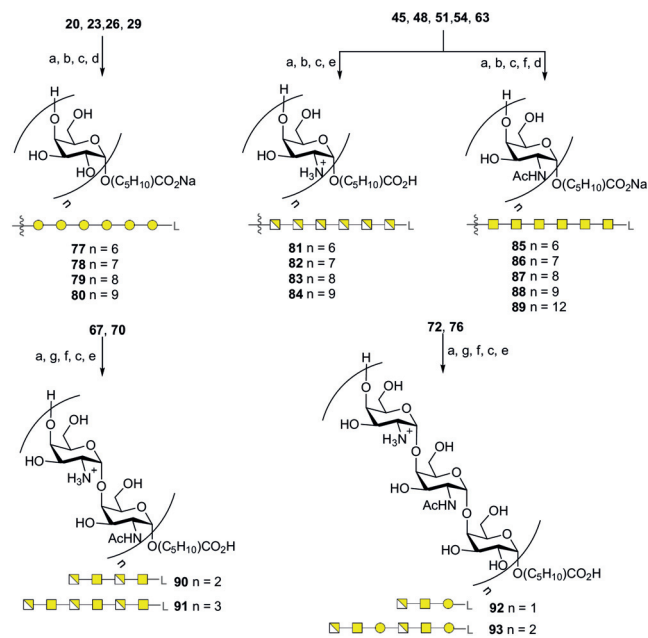
β). The α-linked product was then transformed into the required C-4-OH acceptor using the desilylation-benzoylation sequence as described above. Condensation of the thus formed monomer **64**, with GalN₃ donor **2b** provided the GalN₃-GalNTCA dimer, which was transformed into **65** (80 % yield over three steps). Elongation of this dimer with another copy of the GalNTCA donor **3** and subsequently the GalN₃ building block **2b**, delivered tetrasaccharide **67** in excellent yields. Repetition of these events led to the GalN₃-GalNTCA hexasaccharide **70**. The last members of our GAG-library feature Gal, GalN and GalNAc moieties (Scheme 1B) and donors **1**, **2b** and **3** were used in the above described strategy to assemble these structures. Thus, Gal-monosaccharide **7** was condensed with GalNTCA donor **3** to deliver, after desilylation and benzoylation, the Gal-GalNTCA dimer **71**. Elongation of this dimer with GalN₃ **2b** provided trisaccharide **72** featuring the three structural C-2 modifications. Unmasking the C-4'-OH then set the stage for the elongation of the trisaccharide with subsequently building block **1**, **3** and **2b** leading to the hexasaccharide **76**. Also this last mixed sequence structure was generated uneventfully, showing the chemistry developed to be applicable to any type of GAG-target.

With all protected fragments in hand deprotection conditions were developed to complete the assembly of the GAG library (Scheme 2). First the set of Gal-oligomers was brought to the end stage by removing the silylidene ketal, followed by saponification of the benzoates and benzyl ester, hydrogenolysis of all benzyl ethers and an ion-exchange procedure to furnish the sodium salts of the target com-

pounds. Following this sequence of events, hexasaccharide **77** and heptasaccharide **78** were obtained in 69 % and 75 % yield, respectively. The octasaccharide **79** and nonasaccharide **80** on the other hand were obtained in significantly lower yields (25 % and 29 % respectively), because their solubility in water—quite surprisingly—turned out to be relatively poor.

Next GalN₃ oligomers **45**, **48**, **51**, **54** and **63** were transformed into the set of GalN- and GalNAc-target compounds **81–84** and **85–89**. Similar to the Gal-series, removal of the silylidene groups from these substrates was followed by saponification and reduction of the benzyl esters and azide moieties. An anion ion exchange reaction (to change the acetate counterions for chlorides) delivered the GalN-oligomers **81–84**, all in good yield. No solubility issues were encountered in this series. The free amines generated could also be chemoselectively acetylated to provide the GalNAc-oligosaccharides **85–89**. Also these oligomers proved to be well soluble in water and were obtained as their sodium salts in 39 %–62 % yield (over 5 steps). The GalN₃-GalNTCA tetramer **67** and hexamer **70** were transformed into the GalN-GalNAc tetra- and hexasaccharide **90** and **91**, by removal of the silylidene ketal, saponification of the benzoates, benzyl ester and trichloroacetamides, followed by acetylation of the exposed amines. Removal of the benzyl ethers and reduction of the azides and ion exchange delivered **90** and **91** in 34 % and 44 %, respectively. Finally, the GalN-GalNAc-Gal trisaccharide and hexasaccharide **72** and **76** were generated following the same deprotection sequence to deliver **92** and **93** in 68 % and 65 % yield.

To investigate the conformation and spatial presentation of the synthetic GAGs, their structural properties were studied by a combination of NMR and computational methods.^[9] First, molecular dynamics (MD) simulations were performed (see the Supporting Information for full experimental details), using the GLYCAM and GAFF force fields within the AMBER package, to model the structures of hepta- and nonasaccharides built up from either Gal, GalNAc or GalN residues.^[10] The computed conformational distribution around every Φ/Ψ is close to identical for each glycosidic linkage in the oligomers. For the Gal- and GalNAc-oligosaccharides, the MD simulations predicted an almost equal population of two conformational regions, which differ in Ψ (Ψ⁺ and Ψ[−]). In both geometries Φ fulfills the *exo*-anomeric effect (*exo-syn*, −60°). For the GalN-oligomers, a single population was predicted, close to the Ψ[−] region. Of note, the overall structure of both the Ψ⁺ and Ψ[−] conformers for all three studied homo-oligomers were very similar, with the oligosaccharides taking up an elongated, almost straight structure, with no contacts between non-adjacent residues, and the monomeric constituents stacked above one another (See Figure 2). To provide experimental support for these structures, heptasaccharides **78** (Gal7), **82** (GalN7) and **86** (GalNAc7) were studied by NMR spectroscopy. Key proton–proton inter-residue distances and the possible inter-residue hydrogen bonds (HB) were scrutinized. Interestingly, most of the NMR cross peaks in the HSQC spectra of the heptasaccharides displayed the same or very similar chemical shift, suggesting a very similar chemical environment for the repeating units and thus a regular structure. However, this



Scheme 2. Deprotection of synthesized oligosaccharides. a) HF/pyridine (70 %), THF, 0 °C to rt; b) 1 M NaOH, THF, MeOH; c) Pd(OH)₂/C, THF/H₂O/*t*-BuOH, H₂; d) Dowex-Na⁺, **77**: 69%; **78**: 75%; **79**: 25%; **80**: 29%; **85**: 44%; **86**: 47%; **87**: 46%; **88**: 62%; **89**: 39%. e) Amberlite Cl form, **81**: 67%; **82**: 56%; **83**: 66%; **84**: 55%, **90**: 34%; **91**: 44%; **92**: 68%; **93**: 65%. f) Ac₂O, NaHCO₃, H₂O/THF, g) 2 M NaOH, THF, MeOH.

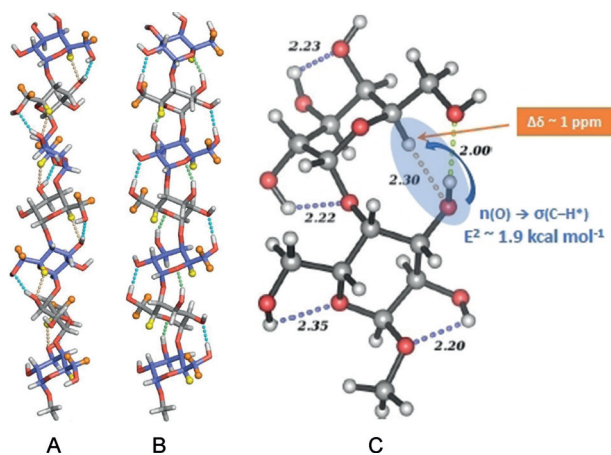


Figure 2. The canonical 3D shapes of the Gal 7-mer. A) The conformer where all Ψ torsion angles show negative values. B) The conformer where all Ψ torsion angles adopt positive values. C) View of the Ψ -conformer for the disaccharide unit with the theoretical HBs. The non-conventional C5-H5($i+1$)...O3(i) HB is highlighted, along with the energy value (ca. 2 kcal mol⁻¹) estimated from the NBO calculations and the expected deshielding for H5 ($\Delta\delta$ ca. 1 ppm).

was not the case for the C5–H5 cross peaks. In particular, δ H5 of the reducing-end residue (1) was around 3.9 ppm, while the chemical shift for the H5 protons of residues 2–7 was around 4.2–4.4 ppm. This significant downfield shift ($\Delta\delta$ 0.3–0.5 ppm) suggests a different chemical environment for H5 at the reducing-end and for H5 at the other residues, with participation of an electron withdrawing entity in the latter with respect to the former case.

NOESY cross peaks were observed between H1($i+1$)/H4(i) and H1($i+1$)/H6_{RS}(i) and key H5($i+1$)/H2(i) NOE cross peaks were also evident. By comparing the NOE-derived distances with the corresponding average ones from MD a very good correlation between the theoretical and experimental values for the H1($i+1$)–H4(i) distances was found. The observed H5($i+1$)–H2(i) NOE is exclusive for the $\Psi+$ conformer, since only this geometry displays these two protons at a NOE-observable distance (ca. 2.6 Å), while they are too far apart in the Ψ -geometry (ca. 3.6 Å). The NOE-derived distance indicated the actual population of the $\Psi+$ conformer to be somewhat larger (60–70%) than that predicted by MD simulations (50%). Overall, the NMR measurements support the structures found by MD and reveal a mixture of $\Psi+$ and $\Psi-$ conformers for the Gal, GalNAc and GalN structures. A major contribution of *gt* and *tg*-rotamers of the hydroxymethyl groups was established, as expected for galactose-type residues.^[11]

To study the inter-residue interactions stabilizing the stacked structures, we studied the Gal-heptamer in detail using quantum mechanical (QM) calculations. Thus, two structures with all *exo-syn*- $\Phi/\Psi-$ or all *exo-syn*- $\Phi/\Psi+$ glycosidic linkages, were built and minimized. For each of them, different HB interactions were repeatedly established along the vicinal residues. For the *exo-syn*- $\Phi/\Psi+$ form, there are HBs between O2($i+1$)...HO6(i) (for the *tg* rotamer) and O5($i+1$)...HO2(i) (Figure 2). For the *exo-syn*- $\Phi/\Psi-$, a HB was found for O6($i+1$)...HO3(i) (for the *gt* rotamer) and a non-

conventional C–H...O HB between C5–H5($i+1$) and O3(i). A similar non-conventional HB has been observed by Schubert et al.^[12] for α 1,3- and α 1,4-L-fucose (Fuc) branched Lewis oligosaccharides. The well-defined 3D-presentation of these molecules is stabilized by a stacking interaction between the Fuc residue and its neighboring branched residue. Because of the non-conventional HB in these structures between the Fuc H5 and the endocyclic O5 of the adjacent sugar residue, the Fuc H5 was shifted downfield by ca. 0.45 ppm.^[12] To further explore this non-conventional HB in the galactose heptamer, natural bond orbital (NBO) and noncovalent interactions analysis (NCI) experiments were carried out.^[13] NBO calculations indeed revealed that one of the lone pairs of O3(i) overlaps with the antibonding C5–H5($i+1$) orbital, providing a favorable contribution of ca. 2 kcal mol⁻¹ (Figure 2). In addition, the NCI analysis clearly detected the interaction (see SI). Since the C5–H5...O3 hydrogen bond could be related to the experimentally observed downfield shift for the H5 protons in the oligosaccharides, the expected δ H5 were calculated employing GIAO-DFT methods. Fittingly, for the *exo-syn*- $\Phi/\Psi-$ models, the computed δ H5 of the non-reducing end (residue 1) was 3.9 ppm, while for the other residues (2–7) δ H5 was between 4.9–5.1 ppm. In contrast, for the *exo-syn*- $\Phi/\Psi+$ conformation, all δ H5 were predicted between 4.0 and 4.2 ppm. The QM-calculations thus support the structures found and explain the difference in chemical shift of the reducing end residue H5 and the protons attached to C5 of residues 2–7. Overall, there is excellent agreement between the MD, NMR and QM-data revealing that the GAG structures adopt a stacked structure, that is stabilized by inter-residue HBs and a non-conventional C–H...O HB. The structure places the C-2 substituents almost perpendicular to the longitudinal axis of the structure on either side of the structure in an alternating fashion.

In conclusion, synthetic methodology enabling the assembly of GAG-oligomers incorporating the possible natural structural variations has been developed. The structures have allowed for detailed structural studies by NMR, assisted by computations.^[14] This revealed that the molecules display elongated, almost straight, geometries, in which the only inter-residue contacts occur between directly linked residues. In these structures, the hydroxymethyl groups and those at C2 (OH/NHAc/NH₂) are presented towards the bulk solvent with an almost perpendicular orientation to the oligosaccharide main chain axis, properly oriented to interact with binding partners, such as biomachinery enzymes or antibodies. DFT calculations indicate a series of inter-residue hydrogen bonds stabilizing both conformations, of which a non-conventional C–H...O HB between H5 of residue ($i+1$) and O3 of residue (i) which was revealed by a significant downfield chemical shift for the non-reducing-end H5 protons in the NMR spectra. This is the first time that this type of non-conventional C–H...O HB is reported for linear oligosaccharide structures. The generated oligosaccharides and established structures can find application in future binding studies to establish GAG-epitopes, that may be used in anti-fungal conjugate vaccine modalities.

Acknowledgements

This work was supported by the European Research Council (ERC-CoG-726072-“GLYCONTROL”, to J.D.C.C. and 788143-RECGLYCANMR-ERC-2017-ADG to J.J.B.) and the Agencia Estatal de Investigación (Spain) (grants RTI2018-094751-B-C21 and SEV-2016-0644).

Conflict of interest

The authors declare no conflict of interest.

Keywords: conformational analysis · glycosylation · non-conventional hydrogen bond · oligosaccharides · stereoselectivity

- [1] a) N. Singh, D. L. Paterson, *Clin. Microbiol. Rev.* **2005**, *18*, 44–69; b) J. Morgan, K. A. Wannemuehler, K. A. Marr, S. Hadley, D. P. Kontoyiannis, T. J. Walsh, S. K. Fridkin, P. G. Pappas, D. W. Warnock, *Med. Mycol.* **2005**, *43*, 49–58; c) G. D. Brown, D. W. Denning, N. A. Gow, S. M. Levitz, M. G. Netea, T. C. White, *Med. Mycol.* **2012**, *4*, 165rv113; d) C. D. Laurushkat, H. Einsele, J. Loeffler, *J. Fungi* **2018**, *4*, 137.
- [2] a) T. Fontaine, A. Delangle, C. Simenel, B. Coddeville, S. J. van Vliet, Y. van Kooyk, S. Bozza, S. Moretti, F. Schwarz, C. Trichot, M. Aebi, M. Delepierre, C. Elbim, L. Romani, J.-P. Latgé, *PLoS Pathog.* **2011**, *7*, e1002372; b) F. N. Gravelat, A. Beauvais, H. Liu, M. J. Lee, B. D. Snarr, D. Chen, W. Xu, I. Kravtsov, C. M. Hoareau, G. Vanier, M. Urb, P. Campoli, Q. Al Abdallah, M. Lehoux, J. C. Chabot, M. C. Ouimet, S. D. Baptista, J. H. Fritz, W. C. Nierman, J. P. Latge, A. P. Mitchell, S. G. Filler, T. Fontaine, D. C. Sheppard, *PLoS Pathog.* **2013**, *9*, e1003575; c) M. S. Gresnigt, S. Bozza, K. L. Becker, L. A. Joosten, S. Abdollahi-Roodsaz, W. B. van der Berg, C. A. Dinarello, M. G. Netea, T. Fontaine, A. De Luca, S. Moretti, L. Romani, J. P. Latge, F. L. van de Veerdonk, *PLoS Pathog.* **2014**, *10*, e1003936; d) N. C. Bamford, B. D. Snarr, F. N. Gravelat, D. J. Little, M. J. Lee, C. A. Zacharias, J. C. Chabot, A. M. Geller, S. D. Baptista, P. Baker, H. Robinson, P. L. Howell, D. C. Sheppard, *J. Biol. Chem.* **2015**, *290*, 27438–27450; e) C. Speth, G. Rambach, C. Lass-Flörl, P. L. Howell, D. C. Sheppard, *Virulence* **2019**, *1–8*; f) C. A. Zacharias, D. C. Sheppard, *Curr. Opin. Microbiol.* **2019**, *52*, 20–26.
- [3] M. J. Lee, F. N. Gravelat, R. P. Cerone, S. D. Baptista, P. V. Campoli, S. I. Choe, I. Kravtsov, E. Vinogradov, C. Creuzenet, H. Liu, A. M. Berghuis, J. P. Latge, S. G. Filler, T. Fontaine, D. C. Sheppard, *J. Biol. Chem.* **2014**, *289*, 1243–1256.
- [4] a) N. C. Bamford, F. Le Mauff, A. S. Subramanian, P. Yip, C. Millan, Y. Zhang, C. Zacharias, A. Forman, M. Nitz, J. D. C. Codee, I. Uson, D. C. Sheppard, P. L. Howell, *J. Biol. Chem.* **2019**, *294*, 13833–13849; b) F. Le Mauff, N. C. Bamford, N. Alnabelseya, Y. Zhang, P. Baker, H. Robinson, J. D. C. Codee, P. L. Howell, D. C. Sheppard, *J. Biol. Chem.* **2019**, *294*, 10760–10772.
- [5] E. D. Kazakova, D. V. Yashunsky, V. B. Krylov, J. P. Bouchara, M. Cornet, I. Valsecchi, T. Fontaine, J. P. Latge, N. E. Nifantiev, *J. Am. Chem. Soc.* **2020**, *142*, 1175–1179.
- [6] a) A. Imamura, H. Ando, S. Korogi, G. Tanabe, O. Muraoka, H. Ishida, M. Kiso, *Tetrahedron Lett.* **2003**, *44*, 6725–6728; b) A. Imamura, H. Ando, H. Ishida, M. Kiso, *Heterocycles* **2008**, *76*, 883–908; c) A. Imamura, H. Ando, H. Ishida, M. Kiso, *Org. Lett.* **2005**, *7*, 4415–4418; d) A. Imamura, A. Kimura, H. Ando, H. Ishida, M. Kiso, *Chem. Eur. J.* **2006**, *12*, 8862–8870; e) A. Imamura, N. Matsuzawa, S. Sakai, T. Udagawa, S. Nakashima, H. Ando, H. Ishida, M. Kiso, *J. Org. Chem.* **2016**, *81*, 9086–9104; f) N. Yagami, A. Imamura, *Rev. Agric. Sci.* **2018**, *6*, 1–20.
- [7] S. Kim, H. Chang, W. J. Kim, *J. Org. Chem.* **1985**, *50*, 1751–1752.
- [8] a) B. Yu, J. Sun, *Chem. Commun.* **2010**, *46*, 4668; b) B. Yu, H. Tao, *Tetrahedron Lett.* **2001**, *42*, 2405.
- [9] a) P. Valverde, J. I. Quintana, J. I. Santos, A. Ardá, J. Jiménez-Barbero, *ACS Omega* **2019**, *4*, 13618–13630; b) A. Gimeno, P. Valverde, A. Ardá, J. Jiménez-Barbero, *Curr. Opin. Struct. Biol.* **2020**, *62*, 22–30.
- [10] D. A. Case, T. E. Cheatham, T. Darden, H. Gohlke, R. Luo, K. M. Merz, A. Onufriev, C. Simmerling, B. Wang, R. J. Woods, *J. Comput. Chem.* **2005**, *26*, 1668–1688.
- [11] a) K. Bock, J. Ø. Duus, *J. Carbohydr. Chem.* **1994**, *13*, 513–543; b) R. Stenutz, I. Carmichael, G. Widmalm, A. S. Serianni, *J. Org. Chem.* **2002**, *67*, 949–958.
- [12] a) T. Aeschbacher, M. Zierke, M. Smieško, M. Collot, J. M. Mallet, B. Ernst, F. H. Allain, M. Schubert, *Chem. Eur. J.* **2017**, *23*, 11598–11610; b) M. Zierke, M. Smieško, S. Rabbani, T. Aeschbacher, B. Cutting, F. H. Allain, M. Schubert, B. Ernst, *J. Am. Chem. Soc.* **2013**, *135*, 13464–13472.
- [13] E. R. Johnson, S. Keinan, P. Mori-Sánchez, J. Contreras-García, A. J. Cohen, W. Yang, *J. Am. Chem. Soc.* **2010**, *132*, 186498–186506.
- [14] A. Ardá, J. Jiménez-Barbero, *Chem. Commun.* **2018**, *54*, 24761–24769.

Manuscript received: March 17, 2020

Accepted manuscript online: April 28, 2020

Version of record online: May 20, 2020